ACS NANO

www.acsnano.org

ARTICLE

Erythrocyte-Mimicking Nanovesicle Targeting *Porphyromonas gingivalis* for Periodontitis

Ying Tang,[§] Yongdan Qi,[§] Yang Chen, Yu-Qiang Wang, Cheng Zhang, Yunxia Sun,* Cui Huang,* and Xian-Zheng Zhang*

Cite This: *ACS Nano* 2024, 18, 21077−21090

Read Online

ACCESS | Metrics & More | Article Recommendations | Supporting Information

ABSTRACT: ***Porphyromonas gingivalis* has been demonstrated to have the strongest association with periodontitis. Within the host, *P. gingivalis* relies on acquiring iron and heme through the aggregation and lysis of erythrocytes, which are important factors in the growth and virulence of *P. gingivalis*. Additionally, the excess obtained heme is deposited on the surface of *P. gingivalis*, protecting the cells from oxidative damage. Based on these biological properties of the interaction between *P. gingivalis* and erythrocytes, this study developed an erythrocyte membrane nanovesicle loaded with gallium porphyrins to mimic erythrocytes. The nanovesicle can target and adhere with *P. gingivalis* precisely, being lysed and utilized by *P. gingivalis* as erythrocytes. Ingested gallium porphyrin replaces iron porphyrin in *P. gingivalis*, causing intracellular metabolic disruption. Deposited porphyrin generates a large amount of reactive oxygen species (ROS) under blue light, causing oxidative damage, and its lethality is enhanced by bacterial metabolic disruption, synergistically killing *P. gingivalis*. Our results demonstrate that this strategy can target and inhibit *P. gingivalis*, reduce its invasion of epithelial cells, and alleviate the progression of periodontitis.**

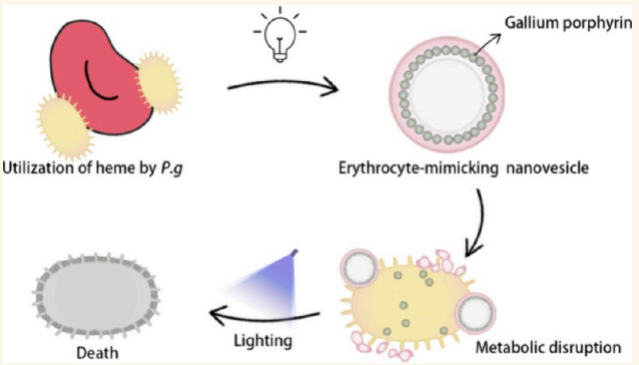

KEYWORDS: *Porphyromonas gingivalis, erythrocyte-mimicking, metabolism, photodynamic therapy, periodontitis*

INTRODUCTION

Periodontitis, a chronic bacterial infectious disease, affects millions of populations every year, resulting in the destruction of periodontal tissue and the loss of teeth.[1−4] In periodontitis subgingival plaque, *P. gingivalis* is the most strongly and consistently associated with chronic periodontitis.[5−7] *P. gingivalis* is located at the nonattached subgingival biofilm in the periodontal pocket,[8] continuously stimulating periodontal tissue, then invading and colonizing in epithelium cells, and inducing the immune and inflammatory response of the host, which causes severe destruction of periodontal tissues.[9,10] Many researchers have found that the invasion of *P. gingivalis* into the human body is related to many diseases such as infective endocarditis, rheumatoid arthritis, and Alzheimer's disease.[11,12] At present, traditional antibiotic therapy fails to achieve satisfactory effects and presents challenges such as resistance of *P. gingivalis* and dysbiosis of oral microbiota.[13,14] Recent studies have shown that *P. gingivalis* is a potential therapeutic target for periodontitis,[15−18] and reducing its abundance in subgingival plaque is beneficial for treating periodontitis.

Notably, iron and heme are critical factors in the growth and virulence of *P. gingivalis*. *P. gingivalis* cannot synthesize these compounds independently and must be obtained from the external environment.[19−22] Within the human host, *P. gingivalis* can acquire heme and iron from hemoglobin by aggregating with erythrocytes through hemagglutinins and lysing them through proteases.[23−25] Once released, heme is broken down by gingipains and other proteases and transported into cells via hemin/hemoglobin receptors, such as HmuR or HmuY.[26,27] Excess heme obtained can be accumulated and deposited on the surface of the bacterium,[28] which exhibits peroxidase activity assists in protecting the bacteria from oxidative damage,[29] and also explains its characteristic black colony phenotype. Overall, *P. gingivalis* can aggregate, lyse red blood cells, and accumulate heme.[30] However, literature reports on periodontitis biomaterials treatment have rarely focused on

Received: February 19, 2024
Revised: July 16, 2024
Accepted: July 19, 2024
Published: August 1, 2024

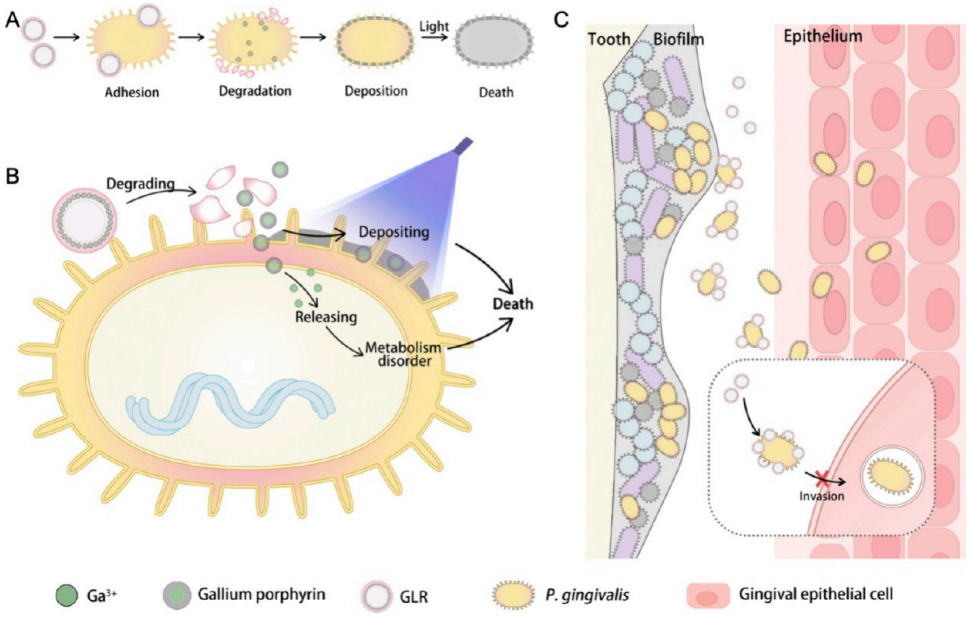

Figure 1. (A) *P. gingivalis* aggregates with GLR and lysates it to acquire gallium porphyrin, which subsequently lead to its death due to metabolism disorder and photodynamic therapy. (B) GLR inhibits *P. gingivalis* by disordering bacterial metabolism and photodynamic. (C) *P. gingivalis* in periodontal pocket is enveloped by GLR, which weakens their invasion of epithelium cells.

these biological characteristics of *P. gingivalis* itself, specifically its adhesion with erythrocytes and its utilization of heme.

Nowadays, erythrocyte-related materials have been applied in the treatment of tumors, cardiovascular disease, brain diseases, and other systemic administration due to their biocompatibility, biodegradability, and long circulation.[31−34] However, interactions between erythrocytes and bacteria have barely received attention. In this study, based on the adhesion between *P. gingivalis* and erythrocytes and its utilization of heme, we constructed erythrocyte-mimicking nanovesicles (an erythrocyte membrane liposome loaded with gallium porphyrin, denoted as GLR) to target *P. gingivalis* precisely. Like an erythrocyte, GLR can adhere to *P. gingivalis* and provide gallium porphyrin. Since bacteria cannot distinguish between iron and gallium ions, the absorption of gallium porphyrin disrupts intracellular metabolism.[35−37] Excess obtained porphyrin deposited on the surface of the bacteria can generate an amount of ROS under photodynamic therapy, which can cooperate with gallium ions for antibacterial effects. In addition, the antibacterial effect can be enhanced by the increased sensitivity of bacteria to oxygen due to metabolic disorders (Figure 1). The results showed that GLR treatment could effectively inhibit *P. gingivalis* and reduce its invasion into epithelial cells. GLR treatment also effectively decreased the proportion of *P. gingivalis* in subgingival plaque, alleviated local inflammation, and inhibited bone resorption in periodontitis rats. We hope that this strategy will provide a different approach to the precise treatment of periodontitis.

RESULTS AND DISCUSSION

Interaction Between Erythrocyte and *P. gingivalis*. According to previous studies,[23,25,26] *P. gingivalis* can adhere to erythrocyte via hemagglutinin, disrupting the erythrocyte membrane, and subsequently utilizing and storing heme on the surface of the bacterium, which is its biological characteristic. Therefore, we first explored the adhesion of *P. gingivalis*, and other common gastrointestinal bacteria, including *Streptococcus mutans*, and *Escherichia coli* Nissle 1917, to explore their ability to adhere to red blood cells. Freshly obtained red blood cells (RBCs) were cocultured with different bacteria, and the result (Figures S1 and 2A) showed that *P. gingivalis* exhibited stronger adhesion to red blood cells than *S. mutans* or *E. coli* Nissle 1917. From Figure 2A, it can be observed that many *P. gingivalis* (blue) adhered to the surface of the erythrocyte (red), gathering into clusters. The transwell assay showed that *P. gingivalis* migrated more readily to heme-containing and RBC-containing medium (Figure 2B,C). These results confirm the interaction between *P. gingivalis* cells and erythrocytes, which is consistent with previous research.[24,26] These also provide inspiration for the construction of *P. gingivalis*-targeted erythrocyte-mimicking nanovesicles.

Design and Characterization of GLR. At present, many studies have shown the advantages of cell membrane-associated nanomaterials in drug delivery.[38,39] The RBC-based drug delivery system has a long circulation time, excellent biocompatibility, and translational application prospects.[32,34,40,41] Based on the fact that *P. gingivalis* has a tendency to adhere to erythrocytes and acquire heme to sustain its growth and virulence (Figure 2D), a liposome containing an RBCs membrane was constructed to target *P. gingivalis* and deliver gallium porphyrin. Since *P. gingivalis* cannot distinguish between iron ions and gallium ions (Figure 2E), gallium porphyrins could be absorbed instead of iron porphyrins, thereby affecting the metabolism of *P. gingivalis*.

First, gallium porphyrin was synthesized according to the literature.[42] The successful synthesis of gallium porphyrin was verified by ^{1}H NMR (Figure S2) and high-resolution mass spectrometry (Figure S3). The synthesized gallium porphyrin has a fluorescence characteristic absorption peak at 580 nm (Figure S4A) and an ultraviolet characteristic absorption peak at 405 nm (Figure S4B), which is consistent with the previous study.[43] In addition, gallium porphyrins exhibit poor water solubility (Figure S5), and using erythrocyte-mimicking

https://doi.org/10.1021/acsnano.4c02316
ACS Nano 2024, 18, 21077−21090

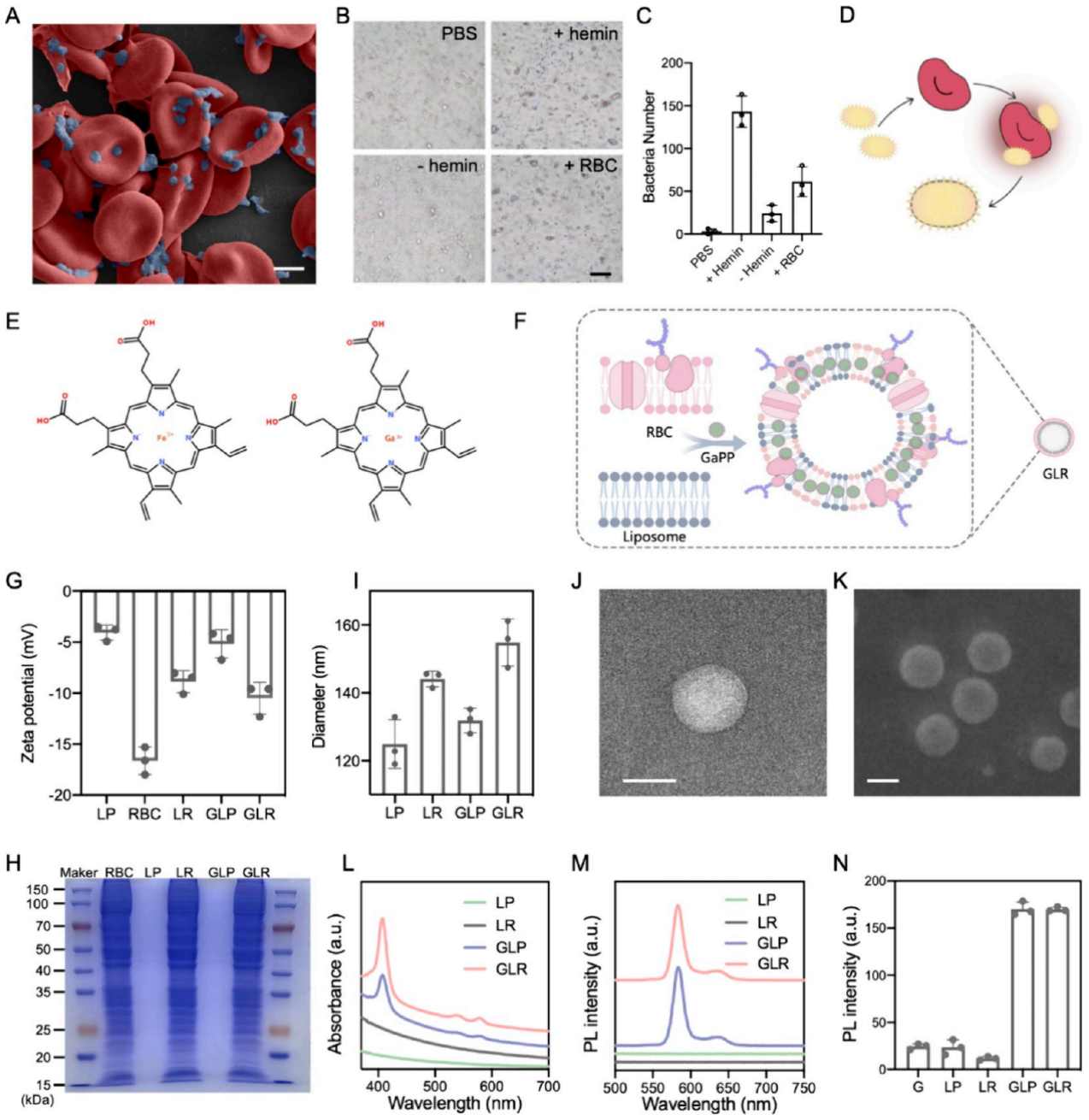

Figure 2. (A) SEM image of *P. gingivalis* adhesion with RBCs (scale bar: 2 μm). (B) Transwell assay images and (C) data analysis of *P. gingivalis* incubated with PBS, medium with hemin, medium without hemin, medium with RBCs (scale bar: 10 μm). (D) Diagram of *P. gingivalis* aggregating with RBCs and utilizing iron porphyrin. (E) Chemical structures of iron porphyrin (left) and gallium porphyrin (right). (F) Illustration of gallium porphyrin (denoted as G) - loaded red blood cell membrane-liposome (GLR). (G) Zeta potential changes during the synthesis of GLR. (H) SDS-PAGE of RBC, LP, LR, GLP, and GLR. (I) Diameter of LP, LR, GLP, and GLR. (J) TEM image and (K) SEM image of GLR (scale bar: 100 nm). (L) UV−vis absorption spectra of LP, LR, GLP, and GLR. (M) Fluorescence spectrum of LP, LR, GLP, and GLR under blue light. (N) Detection of ROS produced after gallium porphyrin (denoted as G), LP, LR, GLP, and GLR under blue light by DCFH.

liposomes to load and deliver gallium porphyrin can enhance the utilization of gallium porphyrin.

Then, according to the literature on cell membrane liposomes,[44] 1,2-dioleoyl-*sn*-glycero-3-phosphocholin (DOPC) was used to synthesize liposome (denoted as LP) and liposome loaded with gallium porphyrins (denoted as GLP). Red blood cell membranes (RBC) were added during the synthesis process of liposomes to synthesize liposome-containing red blood cell membranes (denoted as LR) and liposome-containing red blood cell membranes loaded with gallium porphyrins (denoted as GLR) (Figure 2F). During the synthesis process, there was a notable change in the zeta potential (Figure 2G), which was about -4 mV for LP, −18 mV for RBC, −10 mV for LR, −5 mV for GLP, and −11 mV for GLR. Comparing the results of GLP and GLR in the sodium dodecyl sulfate-polyacrylamide gel electrophoresis (SDS-PAGE) analysis (Figure 2H), it can be found that the erythrocyte membranes fused into GLR, confirming the

https://doi.org/10.1021/acsnano.4c02316
ACS Nano 2024, 18, 21077−21090

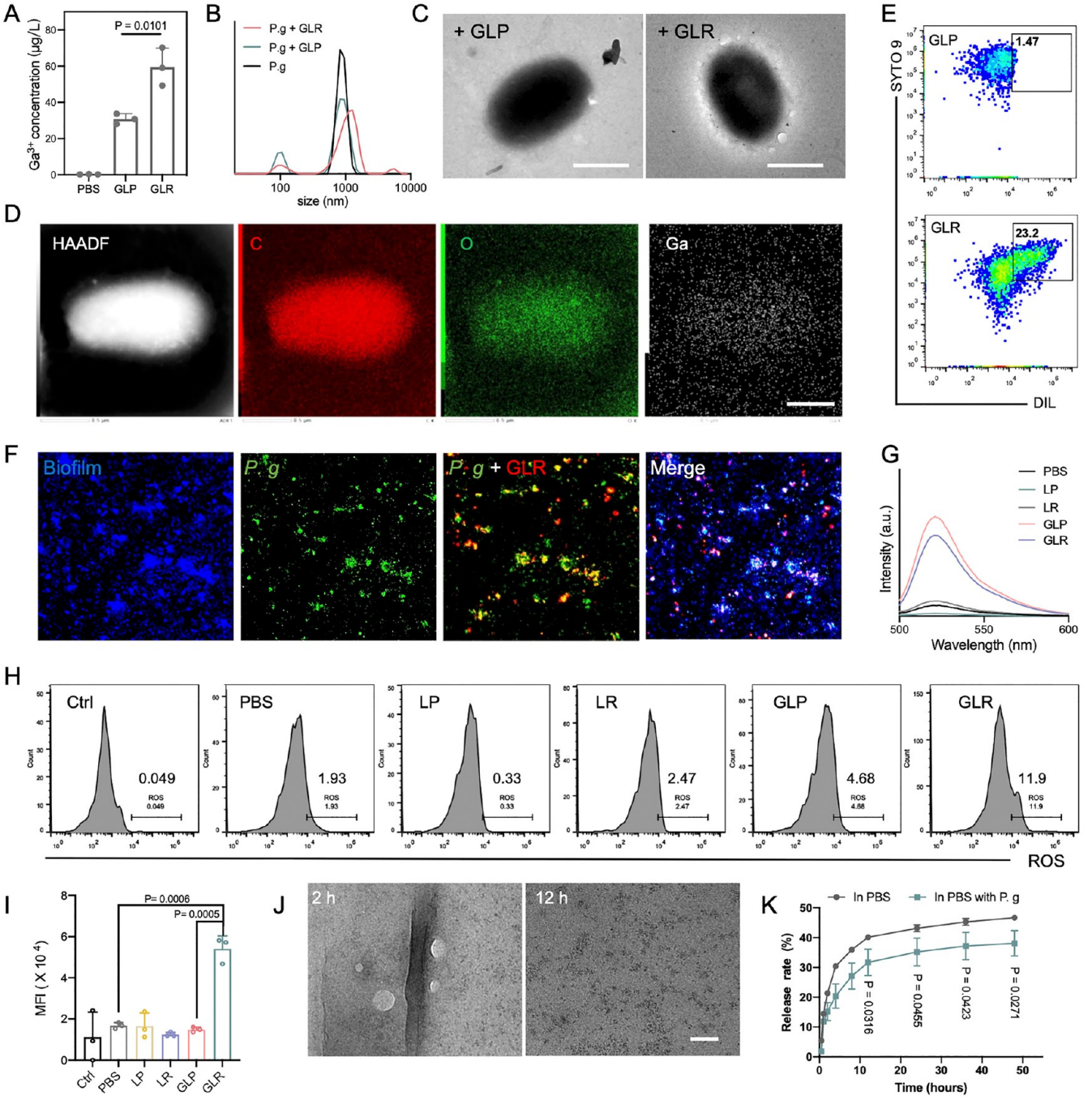

Figure 3. (A) Measurement of Ga^{3+} ion concentration of *P. gingivalis* after incubation with GLP or GLR by ICP analysis. (B) Changes in the diameter of *P. gingivalis* after aggregation with GLP or GLR. (C) TEM images of *P. gingivalis* incubated with GLP or GLR for 30 min (scale bar: 0.5 μm). (D) HAADF-STEM images of *P. gingivalis* incubated with GLR, and distribution of elements C, O, and Ga (scale bar: 0.5 μm). (E) Flow analysis of *P. gingivalis* (labeled SYTO 9) incubated with GLP or GLR (labeled DIL). (F) Fluorescence images of *P. gingivalis* (labeled SYTO 9)-containing biofilm (labeled Hoechst 33342) incubated with GLR (labeled Cy-5.5). (G) Detection of the extracellular ROS production of *P. gingivalis* after incubation with PBS, LP, LR, GLP, and GLR under blue light using DCFH. (H) Flow analysis and (I) fluorescence intensity of intracellular ROS produced in *P. gingivalis* after treatment with PBS, LP, LR, GLP, or GLR under blue light. (J) TEM images of GLR degradation after treatment with the *P. gingivalis* supernatant (scale bar: 100 nm). (K) Release of gallium porphyrin from GLR in PBS or the *P. gingivalis* supernatant.

successful construction of erythrocyte membrane liposomes. Figures 2I–K, S6, and S7 showed the size and polydispersity index (PDI) of GLP and GLR, and the synthesized GLR was approximately 100 nm. The characteristic peaks of gallium porphyrin in GLR were observed by ultraviolet–visible absorption spectrometry and fluorescence spectrometry (Figure 2L, M). According to the standard curve of gallium porphyrin (Figure S8), it is calculated that the encapsulation rate of gallium porphyrins was approximately 70%, and the drug loading rate of GLR was about 13%. In addition, both GLP and GLR were capable of generating significant levels of reactive oxygen species (ROS) under blue light, which was captured by 2′,7′-dichlorodihydrofluorescein (DCFH) (Figure 2N). The above results proved the successful synthesis of GLR.

https://doi.org/10.1021/acsnano.4c02316
ACS Nano 2024, 18, 21077–21090

Additionally, we extracted primary gingival fibroblasts (Figure S9) and then evaluated the potential toxicity of GLR on gingival fibroblasts in vitro and observed no significant impact on cell viability (Figure S10). This could potentially be attributed to the presence of erythrocyte membrane components in GLR, which enhances its biocompatibility.

Adhesion of GLR to *P. gingivalis*. First, we observed the adhesion of GLR to *P. gingivalis* using a high-resolution confocal fluorescence microscope (Figure S11), preliminarily proving that GLR can target *P. gingivalis* in PBS. Then, *P. gingivalis* was centrifugated after being treated with GLP or GLR, and a purplish-black bacterial precipitation was observed in the GLR group (Figure S12), whereas no such phenomenon was observed in the GLP group. The concentration of gallium ions in the bacterial precipitate was determined by ICP analysis (Figure 3A), revealing that the number of gallium ions that adhered to or taken up by *P. gingivalis* in the GLR group was approximately twice as large as that in the GLP group. The particle size of *P. gingivalis* also increased upon mixing with GLR (Figure 3B), and TEM images (Figure 3C) demonstrated the strong adhesion of GLR to *P. gingivalis*, enveloping *P. gingivalis*, while GLP displayed weak adhesion to *P. gingivalis*. Additionally, the HAADF-STEM images showed that there was a small amount of gallium ion aggregation within *P. gingivalis* treated with GLR (Figure 3D), while there was almost no obvious gallium ion aggregation in *P. gingivalis* treated with GLP (Figure S13).

P. gingivalis (labeled green by SYTO 9) was added with GLP or GLR (labeled red by DIL) for 30 min, and flow cytometer analysis revealed that approximately 23.2% of the *P. gingivalis* cells were adhered with GLR, whereas around 1.41% of the *P. gingivalis* cells were adhered with GLP (Figure 3E). Furthermore, to explore the aggregation between GLR and *P. gingivalis* in a more physiological environment, the human subgingival plaque and *P. gingivalis* were cultured to coconstruct biofilm and treated with GLR. Inverted microscope results showed that GLR (Labeled red by DIL) could still aggregate well to *P. gingivalis* (Labeled green by SYTO 9) in the mixed bacterial biofilm (Labeled blue by Hoechst 33342) (Figure 3F). This provides the possibility for GLR to target *P. gingivalis* in subgingival biofilm in a complex environment in vivo.

GLR Producing ROS under Stimulation. Next, we investigated the ability of GLR to stimulate the production of intracellular and extracellular ROS in the treatment of *P. gingivalis*. First, *P. gingivalis* was treated with different materials (PBS, LP, LR, GLP, or GLR), and DCFH was used to detect the produced extracellular ROS. It can be seen that there was no significant difference in the ability of GLP and GLR to produce extracellular ROS (Figure 3G), which may be due to the fact that the gallium porphyrin loaded in GLP or GLR produces ROS under blue light regardless of whether the GLP or GLR was adhered to the surface of the bacterium or was free in solution.

Subsequently, to detect intracellular ROS production in bacteria treated with different materials, *P. gingivalis* was treated with PBS, LP, LR, GLP, or GLR, respectively, and then centrifuged to remove the supernatant. The bacterial precipitates were dispersed in PBS again, and after exposure to blue light, 2′,7′-dichlorodihydrofluorescein diacetate (DCFH-DA) was added to detect intracellular ROS production. Flow analysis showed that the proportion of *P. gingivalis* cells with oxidative stress after GLR treatment (about 11.9%) was higher than that in other control groups (<5%) (Figure 3H), and the mean fluorescence intensity (MFI) of the *P. gingivalis* treated with GLR was also significantly higher than that of the other groups (Figure 3I). This could be attributed to the adhesion of GLR to the surface of *P. gingivalis* cells, and even some gallium porphyrins have already entered the bacteria. Under blue light, in addition to ROS generated by porphyrins themselves, there are also ROS produced by bacterial stress itself. However, the ROS generated in the bacteria was almost negligible compared to the ROS produced in the GLR group.

GLR Degrading with *P. gingivalis*. Studies have already shown that *P. gingivalis* can bind to erythrocytes using hemagglutinins (e.g., HagA), adhesion domains of gingipains (Kgp and HRgpA), and other proteins (e.g., HBP35).[30] Our results also provided evidence of interaction between *P. gingivalis* and erythrocytes. The release of hemolysins and other proteases by *P. gingivalis* can lead to the disruption of the erythrocyte membrane, resulting in the release of hemoglobin. In light of this, we treated GLR with the supernatant of the *P. gingivalis* culture medium or PBS at room temperature to observe the changes in GLR. The results (Figures S14 and S15) showed that the size and PDI of GLR could remain stable over time in PBS, while changes were significant over time in *P. gingivalis* supernatant, especially at 2 and 12 h. From TEM images, the degradation of GLR in the *P. gingivalis* supernatant can be observed (Figure 3J). This phenomenon is similar to the degradation of red blood cells by *P. gingivalis*, indicating that GLR mimicked red blood cells successfully and that *P. gingivalis* can further degrade GLR to utilize gallium porphyrin. Subsequently, the release of gallium porphyrins in GLR with or without *P. gingivalis* in PBS was investigated. The solubility of gallium porphyrin in PBS was determined by ICP to be approximately 15.4 μg/mL (Figure S16), which is much lower than that in methanol. In drug release experiments, the solution outside the dialysis bag was collected at different time points, with its maximum concentration measured to be approximately 1 μg/mL, lower than the maximum solubility of gallium porphyrin in PBS. Then the release of gallium porphyrin was measured by fluorescence emission spectrometry, and the results (Figure 3K) showed that the release of gallium porphyrins in GLR was significantly lower in the presence of *P. gingivalis* than in the absence of *P. gingivalis*. This is likely due to the degradation of GLR and the utilization of gallium porphyrins by *P. gingivalis*, resulting in a decreased release of gallium porphyrins.

Inhibition of GLR on *P. gingivalis*. To investigate the antibacterial effect of GLR on *P. gingivalis*, we first assessed the impact of GLR loaded with different concentrations of gallium porphyrin on the optical density (OD) value of *P. gingivalis*. The results (Figure S17) showed that the inhibitory effect of GLR on *P. gingivalis* was concentration-dependent. When combined with blue light, GLR treatment led to a greater reduction of the OD value of *P. gingivalis*. This suggested that the inhibitory effect of GLR on *P. gingivalis* was greatly enhanced with light conditions. Besides, we investigated the photothermal effect of GLR under the same conditions, and the results (Figure S18) showed that the temperature of GLR increased by about 1 °C after 30 s under blue irradiation. Therefore, we mainly consider the photodynamic effect of gallium porphyrin in the following experiments.

In order to accurately evaluate and compare the inhibitory abilities of different materials against *P. gingivalis*, we treated *P.*

https://doi.org/10.1021/acsnano.4c02316
ACS Nano 2024, 18, 21077−21090

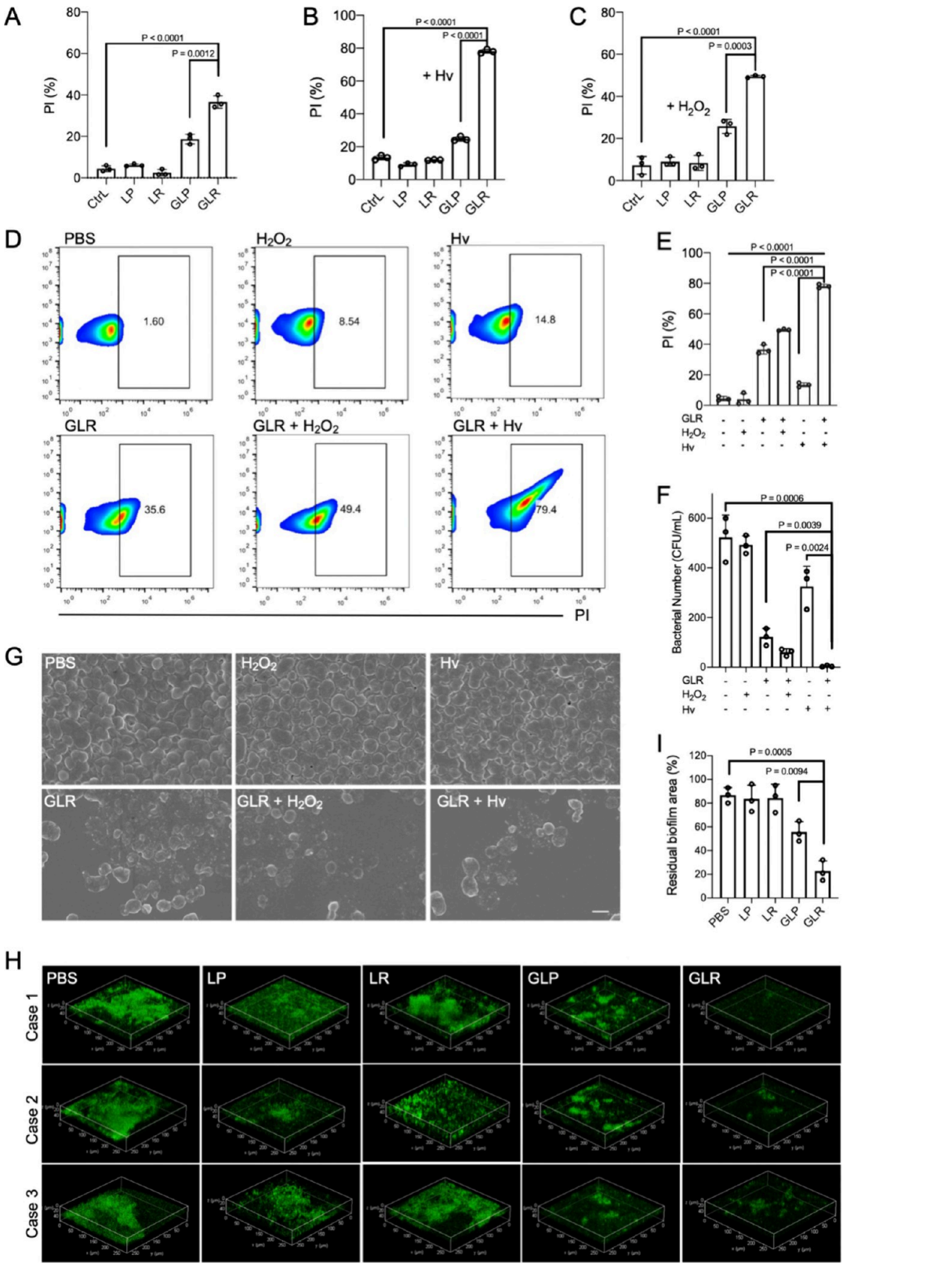

Figure 4. (A) Antibacterial effects of PBS, LP, LR, GLP, or GLR on *P. gingivalis*. (B) Antibacterial effects of PBS, LP, LR, GLP, or GLR on *P. gingivalis* under blue light. (C) Antibacterial effects of PBS, LP, LR, GLP, or GLR on *P. gingivalis* with H_2O_2. (D) Comparison of antibacterial effects and (E) flow analysis of GLR on *P. gingivalis* at different situations. (F) Number and (G) SEM images of *P. gingivalis* treated with GLR under different situations (scale bar: 1 μm). (H) Residual area and (I) relative quantification of biofilm established by human subgingival plaque after treatment with PBS, LP, LR, GLP, or GLR under blue light.

gingivalis with PBS, LP, LR, GLP, or GLR, respectively. Based on the results in Figure S17, the working concentration of gallium porphyrin that we subsequently used was 20 μg/mL, and the proportion of dead bacteria was detected by propidium

https://doi.org/10.1021/acsnano.4c02316
ACS Nano 2024, 18, 21077−21090

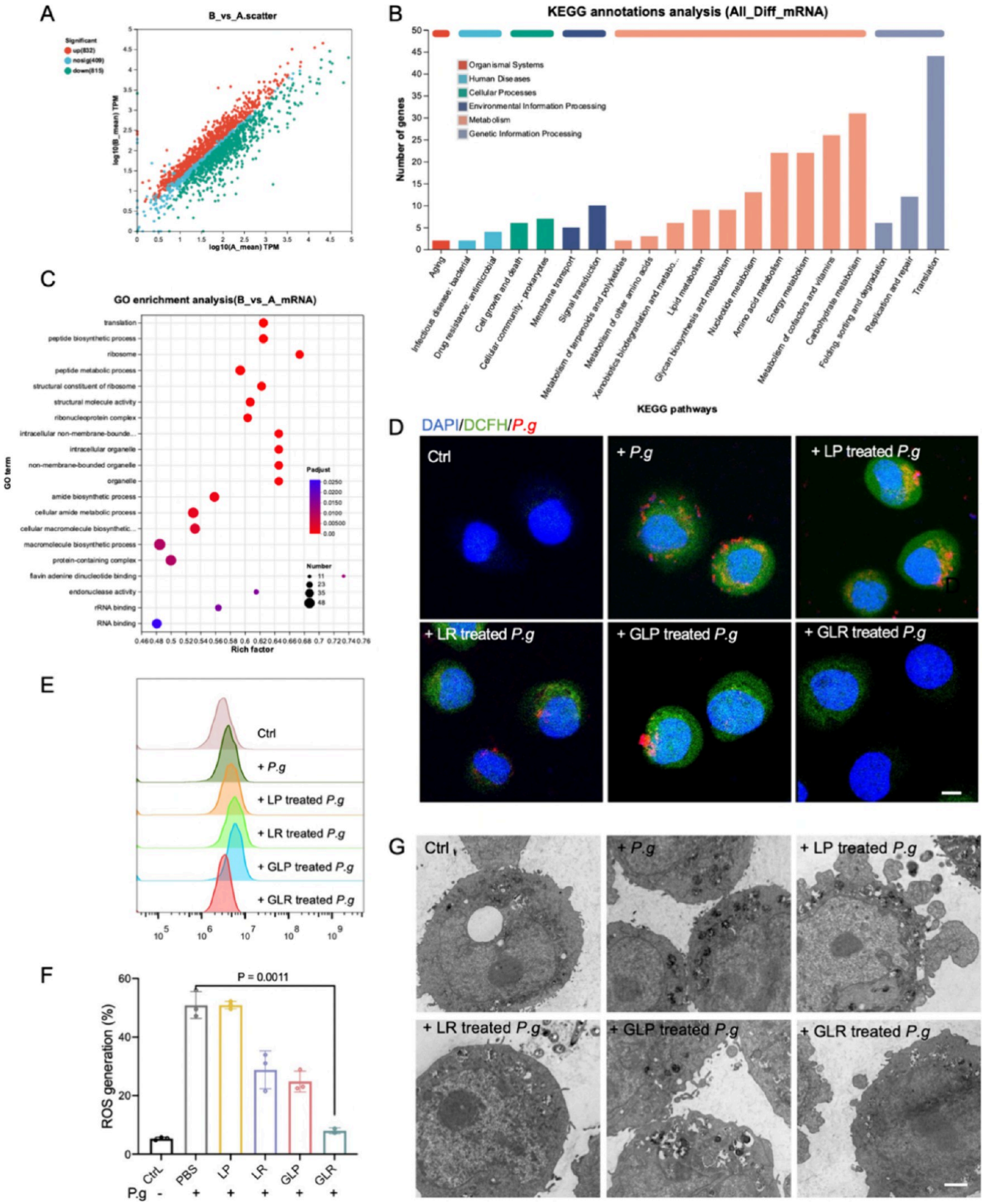

Figure 5. (A) Scatter plots of the number of genes with significant expression differences in *P. gingivalis* after treatment with the GLR as analyzed by RNA-seq (A: ctrl, B: GLR-treated). (B) KEGG annotations analysis, and (C) GO enrichment analysis of *P. gingivalis* after treatment with the GLR(A: ctrl, B: GLR-treated). (D) Confocal microscopy images of the adhesion of *P. gingivalis* with different treatments to epithelial cells. (E) Flow cytometry and (F) quantitative analysis of the amount of ROS produced in the epithelial cells after treatment (scale bar: 5 μm). (G) Electron microscopy images of the invasion of *P. gingivalis* to epithelial cells (scale bar: 2 μm).

https://doi.org/10.1021/acsnano.4c02316
ACS Nano 2024, 18, 21077−21090

iodide (PI) staining and flow cytometry analysis. The results indicated that in the absence of light, the antibacterial effect of GLP and GLR on *P. gingivalis* was approximately 18 and 40%, respectively (Figure 4A). This antimicrobial effect can be attributed to the substitution of iron ions with gallium ions inside the bacteria, disrupting the bacteria's metabolism. While in the presence of light, the inhibition rates of GLP and GLR against *P. gingivalis* approximately increased by 30 and 80%, respectively (Figure 4B). These findings indicate that GLR is more effectively recognized and utilized by *P. gingivalis* compared to GLP, which benefits from the exposure of erythrocyte membrane-associated proteins on the surface of GLR. Furthermore, the utilization of gallium ions is likely to impact bacterial metabolism, while the deposition of porphyrins on the bacterial surface induces the production of ROS under light exposure, ultimately resulting in bacterial death.

Previous studies have shown that for anaerobic bacteria such as *P. gingivalis*, iron porphyrin that is stored on its surface exhibits peroxidase activity based on the transformation of iron and ferrous ions under oxidative stress, protecting the bacterium itself from oxidative damage.[19,30] In addition, metabolically disordered bacteria may possess increased sensitivity to ROS and a decreased ability to regulate oxidative stress. When gallium porphyrin replaces iron porphyrin, the antioxidant capacity of *P. gingivalis* may be affected. Therefore, we further investigated the survival ability of GLR-treated *P. gingivalis* under oxidative stress conditions.

First, we tested the activity of *P. gingivalis* in the presence of hydrogen peroxide (H_2O_2), and the results showed that *P. gingivalis* could still survive well when the concentration of hydrogen peroxide was less than 5 mM (Figure S19). Then, hydrogen peroxide (5 mM) was added to the *P. gingivalis* which was pretreated with different materials. The results showed that the inhibition rates of GLP and GLR on *P. gingivalis* were approximately 22 and 50%, respectively (Figure 4C). However, untreated *P. gingivalis* was initially able to tolerate this concentration of hydrogen peroxide, while the inhibition rates of GLP or GLR alone were only 18 and 40% (Figure 4A), respectively. These results suggested that after treatment with GLR, even low concentrations of hydrogen peroxide can enhance the antibacterial effect. This indicates that GLR treatment significantly weakens the resistance of *P. gingivalis* against oxidative stress. In addition, Figure 4D, E more directly shows that the inhibition effect of GLR combined with the H_2O_2 group on *P. gingivalis* was enhanced (49.4%) compared with that of H_2O_2 (8.5%) or GLR (35.6%) treatment alone, and GLR combined with Hv (Irradiation with light) group on *P. gingivalis* was significantly enhanced (79.4%) compared with that of Hv (14.8%) or GLR (35.6%) treatment alone, which proves that the metabolic disorder caused by gallium ion and the ROS produced by porphyrin worked synergically to effectively kill *P. gingivalis*. In addition, the treated bacteria were counted (Figure 4F) and observed by SEM (Figure 4G), and the results showed that the GLR combined with the Hv group can destroy the structure of *P. gingivalis* and effectively inhibit the growth of *P. gingivalis*.

GLR Removing Plaque Biofilm In Vitro. The effect of GLR against biofilms containing *P. gingivalis* was evaluated. First, the periodontitis subgingival dental plaque was resuscitated and cultured, and then *P. gingivalis* was added to construct a multispecies biofilm. Next, the biofilms were treated overnight with PBS, LP, LR, GLP, or GLR and then under irradiation with blue light. The results showed that GLR treatment was effective in destroying the biofilm structure (80%) compared to the other groups (<50%) (Figure 4H, I). Previous studies have shown that *P. gingivalis* tends to be located in unattached subgingival plaque, which is related to its ability to acquire heme and facilitate its contact and invasion of gingival tissue. Treatment of *P. gingivalis*-containing biofilm with GLR may induce the migration of *P. gingivalis* to areas with high GLR concentration for metabolic needs. This results in metabolic disorders of *P. gingivalis*, while the deposited porphyrins could generate a large amount of reactive oxygen species under blue light, which not only kills *P. gingivalis* but also destroys the integrity of the biofilm structure, thus promoting the removal of biofilms.

GLR Dysregulating the Metabolism of *P. gingivalis*. Studies have highlighted the significance of iron porphyrins in *P. gingivalis*, particularly in energy metabolism, carbohydrate metabolism, and other biological processes.[19,45] To further explore the effects of GLR treatment on *P. gingivalis*, we conducted an RNA transcriptomic analysis. The results revealed significant alterations in *P. gingivalis* after the absorption of gallium porphyrin instead of iron porphyrin. RNA sequencing data showed that there were 832 upregulated differential genes and 815 downregulated differential genes (Figure 5A). Subsequently, we performed GO and KEGG enrichment analysis on these differentially expressed genes. The results revealed that the biological processes such as carbohydrate metabolism, cofactor and vitamins metabolism, energy metabolism, and macromolecule biosynthetic process of *P. gingivalis* were affected after GLR treatment (Figure 5B, C). These findings explain the antibacterial effect of GLR on *P. gingivalis* and validate our previous speculation, confirming that GLR inhibits *P. gingivalis* growth by disrupting its metabolism.

GLR Reducing the Invasion of *P. gingivalis* into Epithelial Cells. As mentioned earlier, *P. gingivalis* resides in the unattached portion of the subgingival plaque directly exposed to the epithelial tissue. Increasing evidence suggests that *P. gingivalis* possesses immune evasion capabilities by invading and even colonizing epithelial cells. Prolonged stimulation by *P. gingivalis* can lead to an excessive local inflammatory response. However, this process fails to effectively eliminate *P. gingivalis* and may instead result in severe inflammation and bone resorption in periodontal tissues. Furthermore, *P. gingivalis* can enter the body through a bleeding site in the gingival tissue, thereby influencing the development of systemic diseases such as cardiovascular disease and atherosclerosis. Consequently, it is imperative to prevent the invasion of *P. gingivalis* in order to inhibit the progression of periodontitis.

In this part, the invasion ability of *P. gingivalis* with different treatments on oral epithelial cells was investigated. For visualization, *P. gingivalis* was labeled with Cy5.5, oral epithelial cells were labeled with DAPI, and intracellular ROS were detected by DCFH-DA. Figure 5D showed how *P. gingivalis* adhered to or invaded epithelial cells and triggered different levels of oxidative stress response after treatment with different materials. In the GLR-treated group, there was a significant reduction in the adhesion of *P. gingivalis* to epithelial cells, whereas *P. gingivalis* still displayed some adhesion or invasion of epithelial cells in other groups. Flow cytometry quantification of intracellular ROS (Figure 5E,F) indicated that oxidative stress of epithelial cells was significantly reduced in the GLR-treated *P. gingivalis* group compared to other treatment groups,

https://doi.org/10.1021/acsnano.4c02316
ACS Nano 2024, 18, 21077−21090

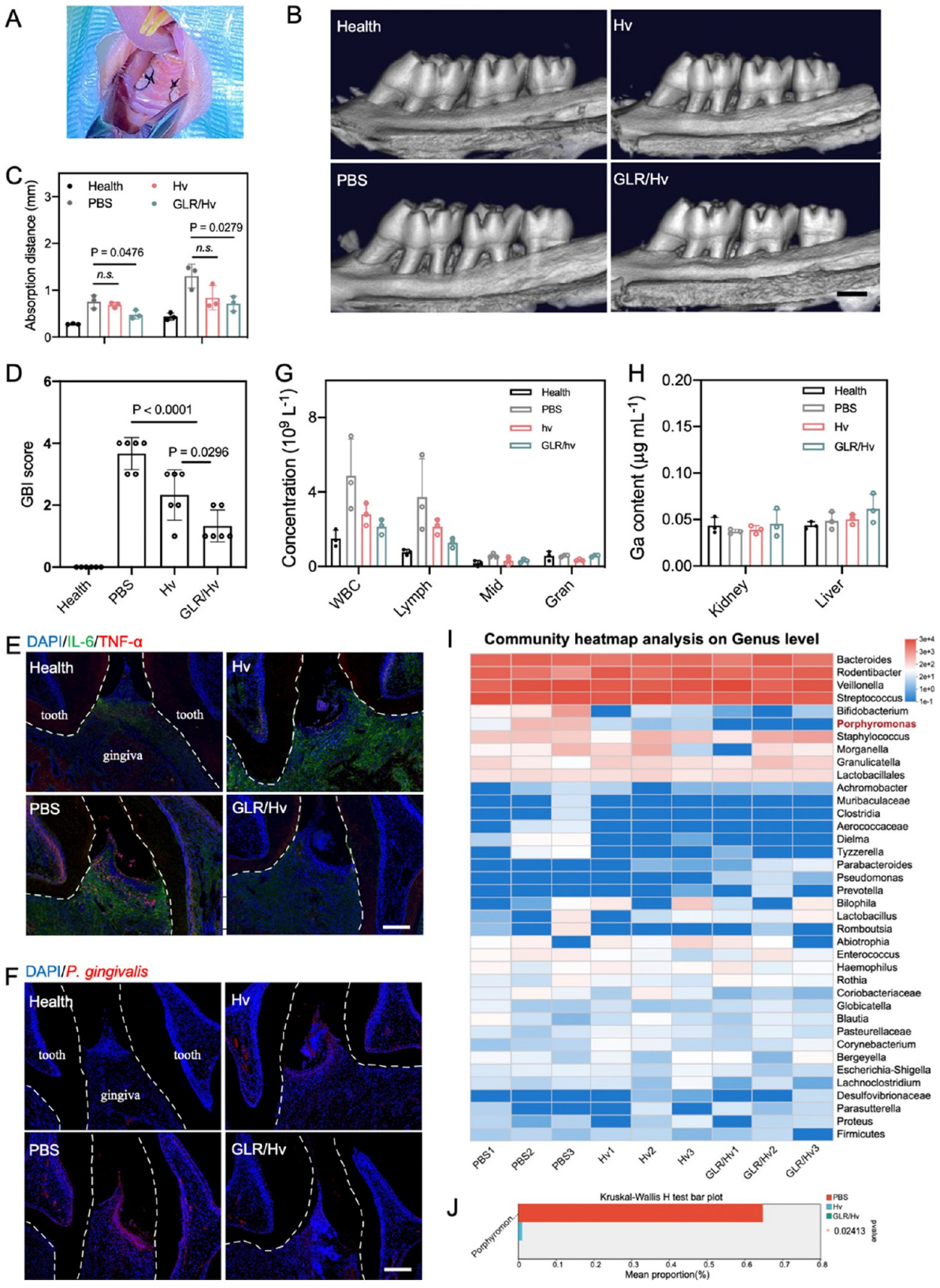

Figure 6. (A) Establishment of the rat periodontitis model through ∞-ligation of the maxillary first molar and second molar. (B) Micro-CT scan 3D reconstruction of rat maxillary ligation area after treatment with PBS, Hv, or GLR/Hv (scale bar: 1 mm). (C) Measurement of the distance of periodontal bone resorption (from alveolar crest to enamelo-cemental junction) after treatments. (D) Assessment of the gingival bleeding index score after treatments. (E) Expression of IL-6 (green) and TNF-α (red) in gingival tissue. (F) Visualization of the location of *P. gingivalis* (red) in gingival tissue by FISH, (scale bar: 200 μm). (G) Routine blood tests of rats after treatments. (H) Measurements of the residual Gallium ions in the liver or kidneys by ICP analysis. (I) Heat map of the proportion of the top 20 bacteria in the subgingival microbial community after treatments. (J) Changes in the *P. gingivalis* proportion in the subgingival microbial community after treatments.

https://doi.org/10.1021/acsnano.4c02316
ACS Nano 2024, 18, 21077−21090

and the LR and GLR-treated *P. gingivalis* groups also showed some effectiveness. The reduced level of oxidative stress in the LR-treated *P. gingivalis* group may be attributed to the competitive binding between LR and *P. gingivalis*, which reduces the contact between *P. gingivalis* and epithelial cells. In the GLP-treated *P. gingivalis* group, the release of gallium porphyrin from GLP also partially inhibits the activity of *P. gingivalis*. In addition, the oxidative stress response of gingival fibroblasts after treatment was also assessed by DCFH-DA, and the results (Figure S20) showed that GLR-treated reduced the oxidative stress induced by *P. gingivalis*. Moreover, Live/Dead staining of gingival fibroblasts (Figure S21) indicated that GLR-treated cells could alleviate the cell damage caused by *P. gingivalis*.

Furthermore, biological transmission electron microscopy was used to observe the invasion of *P. gingivalis* into epithelial cells. As shown in Figure 5G, a substantial amount of bacteria invasion was observed in the PBS group and the LP-treated *P. gingivalis* group, whereas only a small number of bacterial invasions was observed in the LR-treated *P. gingivalis* group and GLP-treated *P. gingivalis* group. In contrast, minimal bacteria invasion occurred within the interior of the epithelial cells in the GLR-treated *P. gingivalis* group. These findings indicated that the GLR strategy can bind to *P. gingivalis* and inhibit its activity, thereby preventing it from contacting and invading the epithelial cells.

GLR Inhibiting the Progress of Rat Periodontitis. To further investigate the effect of GLR in anti-*P. gingivalis* and inhibiting periodontitis in vivo, we established a rat periodontitis model using the ∞-ligation method and inoculated the ligation area with *P. gingivalis* (Figure 6A), which was then treated with PBS, Hv, or GLR combined Hv (GLR/Hv). The results of 3D micro-CT reconstruction (Figure 6B) and statistical analysis (Figure 6C) revealed that GLR/Hv treatment effectively inhibited alveolar bone resorption. Besides, the GBI (gingival bleeding index) scores (Figure 6D) and the expression of inflammatory factors, including IL-6 and TNF-α (Figure 6E) both indicated that GLR/Hv treatment alleviated inflammation in gingival tissues. This may be attributed to the competitive binding of GLR to *P. gingivalis*, which reduces its invasion into the gingival tissues and subsequently alleviates inflammation in periodontal tissues. To visualize the *P. gingivalis* that invaded and survived in gingival tissue, FISH (Fluorescence in situ hybridization) sections were conducted and the results (Figure 6F) suggested that the GLR group exhibited the lowest amount of *P. gingivalis* (red) invasion into the gingival tissues. Besides, the thickness of the gingival epithelium was measured on HE staining sections. As shown in Figure S22, the gingival epithelium thickened in periodontitis compared to healthy gingival, which is likely related to the invasion by *P. gingivalis*, and GLR/Hv treatment reduced the thickening of the gingival epithelium. Additionally, we evaluated markers for neutrophils (MPO), osteoblasts (OCN), and osteoclasts (TRAP). The results (Figures S23−S25) indicate that compared to other groups, there was a decrease in the expression of MPO and TRAP and an increase in the expression of OCN in the GLR/Hv group. These results also supported the conclusion that GLR/Hv treatment can alleviate inflammation in periodontal gingiva and inhibit bone resorption.

In addition, there were no obvious abnormalities in the sections of the vital organs of rats after treatment (Figure S26). The blood routine tests (Figure 6G) showed the white blood cells and lymphocytes in the PBS group were increased, suggesting the existence of inflammation in vivo. In contrast, the blood profiles of GLR/Hv-treated rats were not significantly different from those of healthy rats, suggesting an in vivo antimicrobial effect of GLR/Hv. Importantly, no significant accumulation of gallium ions was detected in the liver or kidneys of the GLR/Hv group through ICP analysis (Figure 6H). These findings demonstrate the potential of the GLR strategy for in vivo applications.

GLR Inhibiting *P. gingivalis* in Subgingival Plaque In Vivo. Periodontal pathogens in subgingival plaque are the initiators of periodontitis; therefore, we investigated the composition of subgingival plaque. The microbial diversity analysis showed that compared with the healthy group (124), the Hv treatment group (98) affected the diversity of oral microbiota to a certain extent, while GLR combined with Hv treatment (110) had a weaker effect on species in subgingival plaque (Figure S27). The Hv treatment reduced the abundance of *P. gingivalis* in the subgingival plaque, which may be related to the use of iron porphyrins in *P. gingivalis*, which is sensitive to blue light. However, the combination of GLR with Hv almost completely eradicated *P. gingivalis* from subgingival plaque (Figure 6I, J). These results suggested that GLR can target *P. gingivalis* and decrease its abundance in periodontitis.

CONCLUSIONS

In this study, a *P. gingivalis*-targeted erythrocyte-mimicking nanovesicle was designed and constructed for periodontitis. This strategy is mainly based on the characteristic properties of *P. gingivalis* binding and lysing red blood cells to obtain iron porphyrin. The erythrocyte-mimicking nanovesicle (GLR) can adhere to and be utilized by *P. gingivalis*, and the gallium porphyrin replaces the iron porphyrin, making the bacteria more sensitive to ROS stimulation. At this time, stimulating porphyrin with blue light to produce ROS can further effectively kill *P. gingivalis*. In vitro experiments showed that GLR could competitively bind to *P. gingivalis* with a high anti-*P. gingivalis* ability and reduce its invasion to epithelial cells. In vivo results showed that GLR could reduce the proportion of *P. gingivalis* in subgingival plaque, reduce its invasion to gingival tissue, alleviate periodontal tissue inflammation, and inhibit bone resorption. Inspired by the results above, we believe that GLR shows promise as a biological material for combating *P. gingivalis* and relieving periodontitis.

EXPERIMENTAL SECTION

Materials. Protoporphyrin dimethyl ester, dimethylpyridine, gallium chloride, and citric acid were purchased from Shanghai Aladdin Biochemical Technology Co., Ltd., and DOPC was obtained from Leyan (Cat.No: 1133946, Shanghai Hao Hong Biological Medicine Technology Co., Ltd.). Chloroform, methanol, ethanol, hydrogen peroxide (30%), and other chemical reagents were purchased from Shanghai Reagent Chemical Co., Ltd. Glutaraldehyde was purchased from Shanghai Maclin Biochemical Technology Co., Ltd; 20 mm glass-bottom dishes and cell culture dishes/plates were obtained from NEST Biotechnology Co.,Ltd. Transwell cell chamber was obtained from SAINING Biotechnology. Gibco α-MEM medium was purchased from Thermo Fisher Scientific Inc. Fetal bovine serum (FBS, BDAA0122-500 mL) were provided by Biodragon (Suzhou, China). Penicillin−streptomycin solution (100×) was purchased from Sperikon Life Science & Biotechnology Co., Ltd. SYTO 9 were obtained from ThermoFisher Scientific Inc., Crystal violet (1%), Hoechst 33342, NHS-Cyanine 5.5 (Cy-5.5) and propidium iodide

https://doi.org/10.1021/acsnano.4c02316
ACS Nano 2024, 18, 21077−21090

(PI) were obtained from Beijing Solarbio Science & Technology Co., Ltd. 1,1′-dioctadecyl-3,3,3′,3′-tetramethylindocarbocyanine perchlorate (DIL), reactive oxygen species detection kit, MTT cell proliferation and cytotoxicity assay kit, and Calcein AM/PI cell activity and cytotoxicity assay kit were provided by Beyotime Biotechnology. Keratinocyte basic medium was obtained from Lonza (China) Investment Co. Ltd.

Incubation of *P. gingivalis*. *P. gingivalis* W83 was obtained from the BeiNa Culture Collection and was cultured according to the ATCC guidelines. The medium contained 30 g/L brain heart infusion, 5 g/L yeast extract, 0.5 g/L cysteine hydrochloride, 0.5 mg/mL hemin, and 0.1 mg/mL vitamin K1. Anaerobically, it was 37 °C.

Erythrocyte Extraction. Whole blood was obtained from healthy female Sprague−Dawley (SD) rats. The erythrocytes were separated by centrifugation (4000 rpm, 5 min) and washed twice with cold phosphate-buffered saline (PBS, pH = 7.4).

Aggregation Between *P. gingivalis* and Erythrocyte. After washing the erythrocyte with PBS, 1 mL (1×10^4/mL) of the erythrocyte was cocultured with different bacteria including *P. gingivalis*, *S. mutans*, and *E. coli* (1×10^8 CFU/mL, 200 μL). After 2 h, the mixture was centrifuged (4000 rpm, 5 min), and the precipitation was washed twice with PBS, fixed with glutaraldehyde (2.5%) for 4 h, then dehydrated with an ethanol gradient, and prepared for scanning electron microscopy (Zeiss SIGMA) observation.

Transwell Assay. After being washed with PBS, *P. gingivalis* (1×10^8 CFU/mL) was dispersed in PBS, and 200 μL of the *P. gingivalis* suspension was placed in the upper chamber of a transwell insert (pore size: 0.4 μm). The lower chamber was filled with different fluids: PBS, culture medium of *P. gingivalis* containing hemin, culture medium of *P. gingivalis* without hemin, and culture medium of *P. gingivalis* containing red blood cells, respectively. The transwell plates were placed in an anaerobic environment and incubated overnight at 37 °C. After the treatment, the bottom of the upper chamber was stained with crystal violet (1%), and the cells were observed and counted by an inverted microscope.

Synthesis of Ga(PPIX)Cl (Gallium Porphyrin). The preparation of Ga(PPIX)Cl was according to the previous literature.[42] Protoporphyrin dimethyl ester (100 mg) was dissolved in dimethylpyridine (6 mL) in a two-necked flask. Gallium chloride (1 g) was suspended in dimethylpyridine (4 mL) and subsequently added dropwise to the flask. The mixture was pumped for 15 min and then heated at 150 °C under an argon atmosphere for 1.5 h. Following cooling to room temperature, the mixture was added to 100 mL of concentrated brine, then acidified to pH = 4 with 20% aqueous citric acid. Finally, the purple precipitate was obtained by filtration and washing with ultrapure water. The collected solid was dissolved in anhydrous methanol, and the solvent was removed by spin evaporation. The resulting product was then subjected to vacuum drying and stored at −20 °C for future experiments.

Extraction of Erythrocyte Membrane. Whole blood was obtained from healthy female SD rats. The erythrocytes were separated by centrifugation (4000 rpm, 5 min) and washed twice with cold phosphate-buffered saline (PBS, pH = 7.4). The washed erythrocytes were suspended in 0.25 x M PBS in an ice bath for 30 min to induce red blood cell rupture. The solution was then centrifuged at 10,000*g* for 10 min to collect the erythrocyte membrane. These rupture and centrifugation treatments were repeated until the precipitate was white. Finally, the erythrocyte membrane was obtained by lyophilization and stored at −80 °C for further use. The above procedures should be conducted on a super clean bench whenever possible.

Synthesize of GLR. Briefly, 3 mL of chloroform was added into a round-bottomed flask and stirred for 10 min. Then, 100 μL of DOPC (10 mg/mL, dissolved in methanol) and 200 μL of Ga(PPIX)Cl (1 mg/mL, dissolved in methanol) were added to the flask drop by drop and stirred at room temperature. After 15 min of stirring (MS7-S magnetic stirrer, DLAB Scientific Co., Ltd) , the lipid membrane was ultrasonically dispersed in 2 mL of HEPES (pH = 7.4) buffer containing 0.32 mg of erythrocyte membrane to form a turbid suspension. Finally, the rehydrated solution was extruded through a 0.4 μm PCTE film, and the unencapsulated Ga(PPIX)Cl was removed by centrifugation (14,000 rpm, 15 min). The above procedures should be conducted on a super clean bench whenever possible.

Characterization of GLR. The potential and particle size of LP, LR, GLP, and GLR were detected by Nano-Zszen 3600 (Malvern Instruments). The particle size and morphology of GLR were observed by scanning electron microscopy (SEM, Zeiss SIGMA) and transmission electron microscopy (TEM, JEM-2100 Plus). The protein on GLR was detected by SDS−PAGE. The UV and fluorescence characteristic peaks of GLR were detected by a fluorescence spectrometer (PerkinElmer) and ultraviolet absorption analyzer (Lambda Bio40, PerkinElmer).

The encapsulation rate of gallium porphyrin (G) was calculated by the following formula: M (loaded G)/M (loaded G + unloaded G) × 100%, and the loading rate was calculated by the following formula: M (G)/M (total) × 100%.

The ROS generation of GLR under blue light was captured by DCFH and detected by a fluorescence spectrometer: In brief, 20 μL of DCFH (20 μM) solution was added to 1 mL of G, LP, LR, GLP, or GLR (same content of DOPC, G: 10 μg/mL) solution, 30 s after blue light irradiation (410 nm, 25 w), and the fluorescence intensities of the solution in different groups were recorded by a fluorescence spectrometer (LS55 luminescence spectrometer, PerkinElmer).

Extraction of Primary Gingival Fibroblasts. The fresh gingival tissues were collected from healthy female rats and immersed in 5 mL of pre-cooled phosphate-buffered saline (PBS) supplemented with 3% penicillin/streptomycin for 5 min. The tissues were then cut into 1 mm 3 pieces, uniformly dispersed in a cell culture dish, and incubated with 8 mL of α-MEM medium in a 5% CO^2 incubator at 37 °C. The medium was replaced with fresh medium every 2 days. When the primary gingival fibroblasts have propagated to 5 mm in diameter around the tissue pieces, the gingival tissue pieces are removed. The primary gingival fibroblasts were collected and cultured for future use.

Cytocompatibility Assay In Vitro. The primary gingival fibroblasts were seeded on a 96-well plate at a density of 1×10^4 and cultured for 24 h. Next, GLR (final concentration of G: 40, 20, 10, 5, 2.5, 1.25, 0 μg/mL) was added and cocultured for 12 h. After that, the medium containing the GLR was removed and replaced with a fresh medium, and incubation was continued for 12 h. The cytocompatibility was evaluated by using an MTT assay. In detail, MTT solution was then added to each well of the 96-well plate for 4 h. The supernatant was replaced with 150 μL of dimethyl sulfoxide (DMSO, Cat. No: 1083196, leyan, shanghai, China), and the optical density (OD) (570 nm) of the solution was observed using a microplate reader (Thermo Scientific Multiskan Go).

Adhesion between *P. gingivalis* and GLR. To evaluate the adhesion between GLR and *P. gingivalis*, 200 μL of GLR (G: 10 μg/mL, labeled by Cy5.5) was added into the solution of *P. gingivalis* (1×10^8 CFU/mL, 200 μL, labeled by SYTO 9). After coincubation for 2 h, the mixture was washed with PBS three times, placed in 20 mm glass-bottom dishes, and observed by high-resolution confocal fluorescence. Besides, 1 mL of *P. gingivalis* (1×10^8 CFU/mL) was centrifugated (6000 rpm, 5 min) and dispersed in 1 mL of PBS, GLP (G: 10 μg/mL), or GLR (G: 10 μg/mL) for 30 min, and then, the bacterial precipitate was obtained by centrifugation (6000 rpm, 5 min). The concentration of gallium ions in the bacterial precipitate was detected by ICP analysis.

Furthermore, 1 mL of *P. gingivalis* (1×10^8 CFU/mL) was dispersed in 1 mL of GLP (G: 10 μg/mL) or GLR (G: 10 μg/mL). After being mixed for 30 min, the bacteria was sampled and detected by Nano-Zszen 3600 and observed by TEM. After being mixed with 4 h, the bacteria were sampled and observed by HAADF-STEM to observe the element distribution of C, O, and Ga.

Next, GLP or GLR was labeled red with DIL, and *P. gingivalis* was labeled green with SYTO 9. Then, 1 mL of *P. gingivalis* (1×10^8 CFU/mL) was dispersed in 1 mL of GLP or GLR (G: 10 μg/mL) for 30 min; after being centrifuged and washed with PBS, the samples were conducted by flow cytometer analysis.

https://doi.org/10.1021/acsnano.4c02316
ACS Nano 2024, 18, 21077−21090

To further explore the aggregation between GLR and *P. gingivalis* in a physiological environment, the periodontitis subgingival dental plaque was resuscitation and cultured to form biofilm and labeled blue with Hoechst 33342, and then, *P. gingivalis* (1×10^8 CFU/mL, 200 μL) labeled green with SYTO 9 was added. After coculturing for 8 h, multispecies plaque biofilm containing *P. gingivalis* was formed, and then, 1 mL of GLR (labeled with DIL, G: 10 μg/mL) was added and incubated for 30 min. After that, the aggregation between GLR and *P. gingivalis* was observed by an inverted microscope.

ROS Intracellular and Extracellular Detection. *P. gingivalis* (1×10^8 CFU/mL, 1 mL) was dispersed in 1 mL of PBS, LP, LR, GLP, or GLR (same content of DOPC, G: 10 μg/mL) for 30 min. After the blue light radiated (410 nm, 25 w, 30 s), the extracellular ROS produced was captured by DCFH and observed using a fluorescence spectrometer. In addition, another group of *P. gingivalis* treated with the above materials was centrifuged to remove the supernatant, and the obtained precipitates were dispersed in PBS and then irradiated with blue light (30 s). The intracellular ROS produced in the bacteria cells were captured by DCFH-DA and measured by flow cytometer analysis.

Degradation of GLR. One milliliter portion of GLR (G: 20 μg/mL) dispersion was added with 200 μL of the *P. gingivalis* culture supernatant or PBS and treated for different times (0, 2, 6, 12, 18, and 24 h) at room temperature. The size and PDI of GLR were analyzed by dynamic light scattering and the mixed solution was sampled and observed by transmission electron microscopy to investigate the status of GLR.

Release of Gallium Porphyrins in GLR. To investigate the release of gallium porphyrins in GLR, the solubility of gallium porphyrins in PBS (37 °C, pH = 7.4) was determined to be 15.4 μg/mL, and the standard curve of gallium porphyrins in PBS was measured by fluorescence emission spectrometry. Then, the prepared GLR (G: 60 μg/mL, 1 mL) was added with 2 mL of PBS that contained *P. gingivalis* (1×10^8 CFU/mL, 200 μL) or not. The 3 mL dispersion was placed in a dialysis bag, which was then placed in a centrifuge tube, and the liquid outside the dialysis bag was 7 mL of PBS. The centrifuge tube was placed on a shaker (100 rpm, 37 °C). The liquid outside the dialysis bag was collected at different time points, and the concentration of gallium porphyrin in the liquid was measured by fluorescence emission spectrometry to calculate the release rate of gallium porphyrin.

Antibacterial Effect Evaluation. First, *P. gingivalis* (1×10^8 CFU/mL, 100 μL) was placed in 96-well plates and treated with different concentrations of GLR (final concentration of G: 40, 20, 10, 5, 2.5, 0 μg/mL). After treatment overnight, the OD values (600 nm) of *P. gingivalis* were observed after applying or not applying blue light.

Next, *P. gingivalis* (1×10^8 CFU/mL, 1 mL) was centrifuged and dispersed in 1 mL of PBS, LP, LR, GLR, or GLR (same content of DOPC, G: 20 μg/mL) respectively. After incubating overnight, blue light was applied for 30 s or not. After treatment, the mixture was stained with PI (5 μg/mL), washed with PBS, and then observed by flow cytometry. Furthermore, the tolerance of *P. gingivalis* to hydrogen peroxide was investigated. *P. gingivalis* (1×10^8 CFU/mL, 1 mL) was centrifuged, and dispersed in 1 mL of culture medium that contained different concentrations of hydrogen peroxide (40, 20, 10, 5, 2.5, 1.25, 0.625, 0 mM), and OD values of *P. gingivalis* were measured after overnight incubation. Then, *P. gingivalis* that pretreated with PBS, LP, LR, GLR, or GLR (same content of DOPC, G: 20 μg/mL) overnight was added with 5 mM hydrogen peroxide. After treatment, the mixture was stained with PI (5 μg/mL), washed with PBS, and then observed by flow cytometry analysis. After treatment with 1 mL of PBS, GLR (G: 20 μg/mL), hydrogen peroxide (5 mM), blue light (30 s), GLR (G: 20 μg/mL) + hydrogen peroxide (5 mM), or GLR (G: 20 μg/mL) + blue light (30 s), the number of *P. gingivalis* was determined by the plate spreading method and the status of *P. gingivalis* was observed using SEM.

Biofilm Formation. In our studies,[46] we collected human subgingival dental plaque samples to construct biofilms, and the plaque samples were cryopreserved. In this section, dental plaque samples were resuscitated using the same medium as that for *P. gingivalis*, and the samples were mixed with *P. gingivalis* (1×10^8 CFU/mL, 200 μL) and inoculated in confocal plates. After 1−2 days of culture, the biofilm visible to the naked eye can be observed at the bottom of the confocal dish. After the biofilms were successfully constructed, 1 mL of PBS, LP, LR, GLP, and GLR were added to the biofilm respectively (the DOPC content was the same, G: 20 μg/mL), and blue light was applied after incubation overnight. The biofilms were stained with SYTO 9 and then observed by Fluorescent confocal microscopy.

RNA Transcriptome Sequencing and Data Analysis. One mL of *P. gingivalis* (1×10^8 CFU/mL) was washed and dispersed in 1 mL of PBS that contained GLR (20 μg/mL) was added for an 8 h treatment. After treatment, the bacteria were centrifuged and rapidly frozen in liquid nitrogen for subsequent sequencing. In brief, total RNA was extracted from bacteria using the CTAB method, and high-quality RNA samples were utilized for subsequent library construction. RNA libraries were constructed using Illumina Stranded mRNA Prep and Ligation from Illumina (San Diego, CA). Double-ended RNA-seq sequencing was performed using Illumina sequencers (NovaSeq6000). The data generated by the Illumina platform were subjected to bioinformatics analysis. All analyses were performed using cloud.majorbio.com, the cloud platform provided by Shanghai Majorbio Biopharm Technology Co., Ltd.

Invasion on Epithelial Cells. Human oral epithelial cells (HOEC) were cultured in a keratinocyte basic medium (KBM) in a 37 °C incubator containing 5% CO_2. The invasion ability of *P. gingivalis* treated with different materials on epithelial cells was evaluated. One milliliter of *P. gingivalis* (1×10^8 CFU/mL, labeled red by NHS-Cy5.5) was pretreated with different materials (PBS, LP, LR, GLP, or GLR (same content of DOPC, G: 20 μg/mL)). HOEC cells were cultured in a T25 cell culture flask for 24 h, and 200 μL of treated *P. gingivalis* was added to HOEC cells for 8 h; then, the cells were stained with DAPI (Cat. No. C3362, APExBIO, Houston, USA), and the intracellular ROS was captured by DCHF-DA. The cells were observed by confocal microscopy, and the produced ROS was quantified by flow cytometry. In addition, the cell precipitate was collected and dispersed in a 2.5% glutaraldehyde solution for bioelectro microscopy.

Periodontitis Model. The establishment of an experimental periodontitis model in rats was based on the previous literature.[46] Briefly, 8-week-old female Sprague−Dawley rats were anesthetized with pentobarbital sodium (30 mg/kg). The rats were placed on a heated operating table. The maxilla and mandible are stabilized in the open position using silk thread, with the maxilla being stabilized more horizontally. The 3−0 sterile silk thread was ligated around the necks of the first and second maxillary molars (M1, M2) using a continuous "∞- ligation" method, and then, 100 μL of *P. gingivalis* (1×10^8 CFU/mL) were orally administrated. Ligature was performed for 7 days, with bandages checked every day. After 24 h of suture, the rats were treated with PBS, Hv, or GLR combined Hv (GLR/Hv). The rats were administered 200 μL of PBS at the ligature site in the PBS group while being administered 200 μL of GLR (G: 60 μg/mL) at the ligature site in the GLR/Hv groups. For Hv treatment, the rats in the Hv and GLR/Hv groups were irradiated with a 410 nm laser (25 w, 30 s). All treatments were repeated twice a day for 7 days. At the end of the experiment, the gingival bleeding index (GBI) was evaluated. Then, the blood of the rats was collected for blood routine analysis (Auto Hematology Analyzer, MC-6200VET), and the maxillary specimens were obtained for CT scanning and histological analysis.

Statistics Analysis. The data were analyzed using GraphPad Prism 7 and SPSS 17.0 software. Results in this study were presented as mean ± SD. Statistical significance between the two groups was assessed by a two-tailed unpaired student's *t-test*, and statistical significance among multiple groups was assessed via one-way analysis of variance (ANOVA).

ASSOCIATED CONTENT

Data Availability Statement

Data will be made available on request.

https://doi.org/10.1021/acsnano.4c02316
ACS Nano 2024, 18, 21077−21090

Supporting Information

The Supporting Information is available free of charge at https://pubs.acs.org/doi/10.1021/acsnano.4c02316.

Details on Materials and Methods, and additional figures including ^{1}H NMR of gallium porphyrin, UV−vis absorption spectra, TEM image, cell viability, HAADF-STEM images, vital organs of rats after treatments, etc (PDF)

AUTHOR INFORMATION

Corresponding Authors

Yunxia Sun − *Key Laboratory of Biomedical Polymers of Ministry of Education & Department of Chemistry, Wuhan University, Wuhan 430072, China*; Email: yx-sun@whu.edu.cn

Cui Huang − *State Key Laboratory of Oral & Maxillofacial Reconstruction and Regeneration, Key Laboratory of Oral Biomedicine Ministry of Education, Hubei Key Laboratory of Stomatology, School & Hospital of Stomatology, Wuhan University, Wuhan 430079, China*; orcid.org/0000-0001-9582-7198; Email: huangcui@whu.edu.cn

Xian-Zheng Zhang − *Key Laboratory of Biomedical Polymers of Ministry of Education & Department of Chemistry, Wuhan University, Wuhan 430072, China*; orcid.org/0000-0001-6242-6005; Email: xz-zhang@whu.edu.cn

Authors

Ying Tang − *State Key Laboratory of Oral & Maxillofacial Reconstruction and Regeneration, Key Laboratory of Oral Biomedicine Ministry of Education, Hubei Key Laboratory of Stomatology, School & Hospital of Stomatology, Wuhan University, Wuhan 430079, China*

Yongdan Qi − *Key Laboratory of Biomedical Polymers of Ministry of Education & Department of Chemistry, Wuhan University, Wuhan 430072, China*

Yang Chen − *State Key Laboratory of Oral & Maxillofacial Reconstruction and Regeneration, Key Laboratory of Oral Biomedicine Ministry of Education, Hubei Key Laboratory of Stomatology, School & Hospital of Stomatology, Wuhan University, Wuhan 430079, China*

Yu-Qiang Wang − *State Key Laboratory of Oral & Maxillofacial Reconstruction and Regeneration, Key Laboratory of Oral Biomedicine Ministry of Education, Hubei Key Laboratory of Stomatology, School & Hospital of Stomatology, Wuhan University, Wuhan 430079, China*

Cheng Zhang − *Key Laboratory of Biomedical Polymers of Ministry of Education & Department of Chemistry, Wuhan University, Wuhan 430072, China*

Complete contact information is available at: https://pubs.acs.org/10.1021/acsnano.4c02316

Author Contributions

[§]Y.T. and Y.Q. contributed equally to this work.

Notes

The authors declare no competing financial interest.

ACKNOWLEDGMENTS

This work was supported by the National Key Research and Development Program of China (2019YFA0905603), the National Natural Science Foundation of China (52333004, 22135005, 82271010 and 82301154), Fundamental Research Funds for the Central Universities (2042023kf0149), and the Interdisciplinary Research Project of School of Stomatology Wuhan University (XNJC202307). Animal experiments were approved by the School and Hospital of Stomatology of Wuhan University Medical Ethics Committee (Approval number: S07923080H).

REFERENCES

(1) Eke, P. I.; Borgnakke, W. S.; Genco, R. J. Recent Epidemiologic Trends in Periodontitis in the USA. *Periodontol. 2000* **2020**, *82*, 257−267.

(2) Slots, J. Periodontitis: Facts, Fallacies and the Future. *Periodontol. 2000* **2017**, *75*, 7−23.

(3) Trindade, D.; Carvalho, R.; Machado, V.; Chambrone, L.; Mendes, J. J.; Botelho, J. Prevalence of Periodontitis in Dentate People between 2011 and 2020: A Systematic Review and Meta-Analysis of Epidemiological Studies. *J. Clin. Periodontol.* **2023**, *50*, 604−626.

(4) Orlandi, M.; Muñoz Aguilera, E.; Marletta, D.; Petrie, A.; Suvan, J.; D'Aiuto, F. Impact of the Treatment of Periodontitis on Systemic Health and Quality of Life: A Systematic Review. *J. Clin. Periodontol.* **2022**, *49* (Suppl. 24), 314−327.

(5) How, K. Y.; Song, K. P.; Chan, K. G. Porphyromonas Gingivalis: An Overview of Periodontopathic Pathogen below the Gum Line. *Front. Microbiol.* **2016**, *7*, 53.

(6) Mysak, J.; Podzimek, S.; Sommerova, P.; Lyuya-Mi, Y.; Bartova, J.; Janatova, T.; Prochazkova, J.; Duskova, J. Porphyromonas Gingivalis: Major Periodontopathic Pathogen Overview. *J. Immunol. Res.* **2014**, *2014*, No. 476068.

(7) Lamont, R. J.; Jenkinson, H. F. Life Below the Gum Line: Pathogenic Mechanisms of Porphyromonas Gingivalis. *Microbiol. Mol. Biol. Rev.* **1998**, *62*, 1244−1263.

(8) Kinane, D. F.; Galicia, J. C.; Gorr, S. U.; Stathopoulou, P. G.; Benakanakere, M. P. Gingivalis Interactions with Epithelial Cells. *Front. Biosci.* **2008**, *13*, 966−984.

(9) Lamont, R. J.; Chan, A.; Belton, C. M.; Izutsu, K. T.; Vasel, D.; Weinberg, A. Porphyromonas Gingivalis Invasion of Gingival Epithelial Cells. *Infect. Immun.* **1995**, *63*, 3878−3885.

(10) Zheng, S.; Yu, S.; Fan, X.; Zhang, Y.; Sun, Y.; Lin, L.; Wang, H.; Pan, Y.; Li, C. Porphyromonas Gingivalis Survival Skills: Immune Evasion. *J. Periodontal Res.* **2021**, *56*, 1007−1018.

(11) Hajishengallis, G. Periodontitis: From Microbial Immune Subversion to Systemic Inflammation. *Nat. Rev. Immunol.* **2015**, *15*, 30−44.

(12) Hajishengallis, G.; Chavakis, T. Local and Systemic Mechanisms Linking Periodontal Disease and Inflammatory Comorbidities. *Nat. Rev. Immunol.* **2021**, *21*, 426−440.

(13) Ardila, C. M.; López, M. A.; Guzmán, I. C. High Resistance against Clindamycin, Metronidazole and Amoxicillin in Porphyromonas Gingivalis and Aggregatibacter Actinomycetemcomitans Isolates of Periodontal Disease. *Med. Oral Patol. Oral Cir. Bucal.* **2009**, *15*, e947−951.

(14) Rams, T. E.; Sautter, J. D.; van Winkelhoff, A. J. Emergence of Antibiotic-Resistant Porphyromonas Gingivalis in United States Periodontitis Patients. *Antibiotics* **2023**, *12*, 1584.

(15) Sundaram, K.; Miller, D. P.; Kumar, A.; Teng, Y.; Sayed, M.; Mu, J.; Lei, C.; Sriwastva, M. K.; Zhang, L.; Yan, J.; Merchant, M. L.; He, L.; Fang, Y.; Zhang, S.; Zhang, X.; Park, J. W.; Lamont, R. J.; Zhang, H. G. Plant-Derived Exosomal Nanoparticles Inhibit Pathogenicity of Porphyromonas Gingivalis. *iScience* **2019**, *21*, 308−327.

(16) Yan, N.; Xu, J.; Liu, G.; Ma, C.; Bao, L.; Cong, Y.; Wang, Z.; Zhao, Y.; Xu, W.; Chen, C. Penetrating Macrophage-Based Nanoformulation for Periodontitis Treatment. *ACS Nano* **2022**, *16*, 18253−18265.

(17) Bai, L.; Shi, E.; Li, Y.; Yang, M.; Li, C.; Li, C.; Wang, Y.; Wang, Y. Oxyhemoglobin-Based Nanophotosensitizer for Specific and Synergistic Photothermal and Photodynamic Therapies against

Porphyromonas Gingivalis Oral Infection. *ACS Biomater. Sci. Eng.* **2023**, *9*, 485−497.
(18) Sun, Q.; Song, W.; Gao, Y.; Ding, R.; Shi, S.; Han, S.; Li, G.; Pei, D.; Li, A.; He, G. A Telluroviologen-Anchored Tetraphenylporphyrin as Sonosensitizer for Periodontitis Sonodynamic Therapy. *Biomaterials* **2024**, *304*, No. 122407.
(19) Olczak, T.; Simpson, W.; Liu, X.; Genco, C. A. Iron and Heme Utilization in Porphyromonas Gingivalis. *FEMS Microbiol. Rev.* **2005**, *29*, 119−144.
(20) Shoji, M.; Shibata, Y.; Shiroza, T.; Yukitake, H.; Peng, B.; Chen, Y.-Y.; Sato, K.; Naito, M.; Abiko, Y.; Reynolds, E. C.; Nakayama, K. Characterization of Hemin-Binding Protein 35 (HBP35) in Porphyromonas Gingivalis: Its Cellular Distribution, Thioredoxin Activity and Role in Heme Utilization. *BMC Microbiol.* **2010**, *10*, 152.
(21) Śmiga, M.; Ślęzak, P.; Wagner, M.; Olczak, T. Interplay between Porphyromonas Gingivalis Hemophore-Like Protein HmuY and Kgp/RgpA Gingipains Plays a Superior Role in Heme Supply. *Microbiol. Spectrum* **2023**, *11* (2), No. e0459322.
(22) Śmiga, M.; Ślęzak, P.; Olczak, T. Comparative Analysis of Porphyromonas Gingivalis A7436 and ATCC 33277 Strains Reveals Differences in the Expression of Heme Acquisition Systems. *Microbiol. Spectrum* **2024**, *12* (3), No. e0286523.
(23) Shah, H. N.; Gharbia, S. E. Lysis of Erythrocytes by the Secreted Cysteine Proteinase of Porphyromonas Gingivalis W83. *FEMS Microbiol. Lett.* **1989**, *52*, 213−217.
(24) Belstrøm, D.; Holmstrup, P.; Damgaard, C.; Borch, T. S.; Skjødt, M. O.; Bendtzen, K.; Nielsen, C. H. The Atherogenic Bacterium Porphyromonas Gingivalis Evades Circulating Phagocytes by Adhering to Erythrocytes. *Infect. Immun.* **2011**, *79*, 1559−1565.
(25) Aleksijević, L. H.; Aleksijević, M.; Škrlec, I.; Šram, M.; Šram, M.; Talapko, J. Porphyromonas Gingivalis Virulence Factors and Clinical Significance in Periodontal Disease and Coronary Artery Diseases. *Pathogens* **2022**, *11*, 1173.
(26) Sakai, E.; Naito, M.; Sato, K.; Hotokezaka, H.; Kadowaki, T.; Kamaguchi, A.; Yamamoto, K.; Okamoto, K.; Nakayama, K. Construction of Recombinant Hemagglutinin Derived from the Gingipain-Encoding Gene of Porphyromonas Gingivalis, Identification of Its Target Protein on Erythrocytes, and Inhibition of Hemagglutination by an Interdomain Regional Peptide. *J. Bacteriol.* **2007**, *189*, 3977−3986.
(27) Olczak, T.; Sroka, A.; Potempa, J.; Olczak, M. Porphyromonas Gingivalis HmuY and HmuR: Further Characterization of a Novel Mechanism of Heme Utilization. *Arch. Microbiol.* **2008**, *189*, 197−210.
(28) Jain, S.; Darveau, R. P. Contribution of Porphyromonas Gingivalis Lipopolysaccharide to Periodontitis. *Periodontol. 2000* **2010**, *54*, 53−70.
(29) Henry, L. G.; McKenzie, R. M. E.; Robles, A.; Fletcher, H. M. Oxidative Stress Resistance in Porphyromonas Gingivalis. *Future Microbiol.* **2012**, *7*, 497−512.
(30) Smalley, J. W.; Olczak, T. Heme Acquisition Mechanisms of Porphyromonas Gingivalis − Strategies Used in a Polymicrobial Community in a Heme-Limited Host Environment. *Mol. Oral Microbiol.* **2017**, *32*, 1−23.
(31) Gao, F.; Tang, Y.; Liu, W. L.; Zou, M. Z.; Huang, C.; Liu, C. J.; Zhang, X. Z. Intra/Extracellular Lactic Acid Exhaustion for Synergistic Metabolic Therapy and Immunotherapy of Tumors. *Adv. Mater.* **2019**, *31*, No. 1904639.
(32) Wang, Y.; Zhang, K.; Qin, X.; Li, T.; Qiu, J.; Yin, T.; Huang, J.; McGinty, S.; Pontrelli, G.; Ren, J.; Wang, Q.; Wu, W.; Wang, G. Biomimetic Nanotherapies: Red Blood Cell Based Core−Shell Structured Nanocomplexes for Atherosclerosis Management. *Adv. Sci.* **2019**, *6*, No. 1900172.
(33) Liang, H.; Huang, K.; Su, T.; Li, Z.; Hu, S.; Dinh, P. U.; Wrona, E. A.; Shao, C.; Qiao, L.; Vandergriff, A. C.; Hensley, M. T.; Cores, J.; Allen, T.; Zhang, H.; Zeng, Q.; Xing, J.; Freytes, D. O.; Shen, D.; Yu, Z.; Cheng, K. Mesenchymal Stem Cell/Red Blood Cell-Inspired Nanoparticle Therapy in Mice with Carbon Tetrachloride-Induced Acute Liver Failure. *ACS Nano* **2018**, *12*, 6536−6544.
(34) Nguyen, P. H. D.; Jayasinghe, M. K.; Le, A. H.; Peng, B.; Le, M. T. N. Advances in Drug Delivery Systems Based on Red Blood Cells and Their Membrane-Derived Nanoparticles. *ACS Nano* **2023**, *17*, 5187−5210.
(35) Olczak, T.; Maszczak-Seneczko, D.; Smalley, J. W.; Olczak, M. Gallium(III), Cobalt(III) and Copper(II) Protoporphyrin IX Exhibit Antimicrobial Activity against Porphyromonas Gingivalis by Reducing Planktonic and Biofilm Growth and Invasion of Host Epithelial Cells. *Arch. Microbiol.* **2012**, *194*, 719−724.
(36) Xie, T.; Qi, Y.; Li, Y.; Zhang, F.; Li, W.; Zhong, D.; Tang, Z.; Zhou, M. Ultrasmall Ga-ICG Nanoparticles Based Gallium Ion/Photodynamic Synergistic Therapy to Eradicate Biofilms and against Drug-Resistant Bacterial Liver Abscess. *Bioact. Mater.* **2021**, *6* (11), 3812−3823.
(37) Huang, K.; Wang, J.; Zhang, Q.; Yuan, K.; Yang, Y.; Li, F.; Sun, X.; Chang, H.; Liang, Y.; Zhao, J.; Tang, T.; Yang, S. Sub 150 Nm Nanoscale Gallium Based Metal−Organic Frameworks Armored Antibiotics as Super Penetrating Bombs for Eradicating Persistent Bacteria. *Adv. Funct. Mater.* **2022**, *32*, No. 2204906.
(38) Han, Z. Y.; Bai, X. F.; Wang, Y. Z.; Chen, Q. W.; Zhang, X. Z. Gut Microbial Glucuronidase-Responsive Glycyrrhizin Micelles for Enhanced Colon Cancer Chemotherapy. *Acta Polym. Sin.* **2022**, *53*, 626−635.
(39) Li, M. J.; Gao, F.; Huang, Q. X.; Feng, J.; Liu, C. J.; Gong, S. L.; Zhang, X. Z. Natural Killer Cell-Mimicking Nanomaterial for Overcoming the Multidrug Resistance of Tumor via Cascade Catalysis. *Sci. China Mater.* **2023**, *66*, 1215−1226.
(40) Liao, J.; Gong, L.; Xu, Q.; Wang, J.; Yang, Y.; Zhang, S.; Dong, J.; Lin, K.; Liang, Z.; Sun, Y.; Mu, Y.; Chen, Z.; Lu, Y.; Zhang, Q.; Lin, Z. Revolutionizing Neurocare: Biomimetic Nanodelivery Via Cell Membranes. *Adv. Mater.* **2024**, *36*, No. 2402445.
(41) Zhu, J.; Xie, R.; Gao, R.; Zhao, Y.; Yodsanit, N.; Zhu, M.; Burger, J. C.; Ye, M.; Tong, Y.; Gong, S. Multimodal Nano-immunotherapy Engages Neutrophils to Eliminate Staphylococcus Aureus Infections. *Nat. Nanotechnol.* **2024**.
(42) Bohle, D. S.; Dodd, E. L.; Pinter, T. B. J.; Stillman, M. J. Soluble Diamagnetic Model for Malaria Pigment: Coordination Chemistry of Gallium(III) Protoporphyrin-IX. *Inorg. Chem.* **2012**, *51*, 10747−10761.
(43) Morales-De-Echegaray, A. V.; Maltais, T. R.; Lin, L.; Younis, W.; Kadasala, N. R.; Seleem, M. N.; Wei, A. Rapid Uptake and Photodynamic Inactivation of Staphylococci by Ga(III)-Protoporphyrin IX. *ACS Infect. Dis.* **2018**, *4*, 1564−1573.
(44) Liu, L.; Pan, D.; Chen, S.; Martikainen, M. V.; Kårlund, A.; Ke, J.; Pulkkinen, H.; Ruhanen, H.; Roponen, M.; Käkelä, R.; Xu, W.; Wang, J.; Lehto, V. P. Systematic Design of Cell Membrane Coating to Improve Tumor Targeting of Nanoparticles. *Nat. Commun.* **2022**, *13*, 6181.
(45) Anaya-Bergman, C.; Rosato, A.; Lewis, J. P. Iron- and Hemin-Dependent Gene Expression of Porphyromonas Gingivalis. *Mol. Oral Microbiol.* **2015**, *30*, 39−61.
(46) Tang, Y.; Huang, Q. X.; Zheng, D. W.; Chen, Y.; Ma, L.; Huang, C.; Zhang, X. Z. Engineered Bdellovibrio Bacteriovorus: A Countermeasure for Biofilm-Induced Periodontitis. *Mater. Today* **2022**, *53*, 71−83.

https://doi.org/10.1021/acsnano.4c02316
ACS Nano 2024, 18, 21077−21090